The *hkl* dependences of microstrain and of macrostress-induced macrostrain; a comparison for intrinsically extremely anisotropic cementite, Fe₃C

A. Leineweber[*], T. Gressmann, M. Nikolussi, E. J. Mittemeijer

Max Planck Institute for Metals Research, Heisenbergstr. 3, 70569 Stuttgart, Germany
[*]a.leineweber@mf.mpg.de

Abstract. On the basis of X-ray diffraction analysis performed on polycrystalline cementite (Fe₃C) layers grown on α-iron substrates, a distinctly positive correlation of the macrostrain (as revealed by the sample-tilting angle dependent peak positions) and of the microstrain (as revealed by the corresponding peak broadening) pertaining to different *hkl*, respectively, was observed. In fact, the *hkl* dependences of both quantities are similar. This can be understood by the strong dependences of both macro- and microstrain on some average values of the (anisotropic) elastic constants along the diffraction vector.

Introduction

Macrostressed polycrystalline thin surface layers (i.e. subjected to mechanical stress) will in case of intrinsic elastic anisotropy and variable grain orientation also exhibit microstrain. Whereas the macrostrain leads to typical sample-orientation peak shifting, the microstrain distribution will lead to broadening of the diffraction peaks. Macrostrain and microstrain may provide valuable information about the overall state of stress/strain in the layer, i.e. the average values *and* the distributions, see e.g. [1]. However, most macrostress studies by diffraction techniques, e.g. using the $\sin^2\psi$-method [2], do not consider the line broadening of the diffraction peaks. That may be partly due to the often relatively large instrumental broadening of the diffractometers dedicated to (macro)stress analysis, masking the structural line broadening.

In the course of X-ray diffraction (macro)stress measurements performed on cementite (Fe₃C) layers grown on α-iron substrates using gaseous nitrocarburising [3], the instrumental configuration was chosen such to allow combining the possibility for specimen tilting with high instrumental resolution. The results of the macrostress analysis were published previously [4]. The present work addresses the state of microstrain in the Fe₃C layer, in particular

with reference to the state of (elastic) macrostrain. At first, in section "Macrostrains and microstrains", the effect of single-crystal elastic anisotropy both on the anisotropic macrostrain and on the anisotropic microstrain is discussed. This serves as basis for the data evaluation in section "Results and discussion".

Macrostrains and microstrains

Consider a rigid substrate with a thin surface layer, which exhibits in the plane parallel to the surface isotropic residual macrostress $\sigma_{\parallel}$. For a given hkl the macrostress leads to a ψ-dependent peak(-centroid) shift with respect to the position pertaining to the strain-free state (index 0). From this shift the corresponding (average) hkl- and ψ-dependent elastic macrostrain $\langle\Delta\varepsilon_{hkl}(\psi)\rangle$ can be calculated according to:

$$\langle\Delta(2\theta_{hkl}(\psi))\rangle = \langle 2\theta_{hkl}(\psi)\rangle - 2\theta_{0,hkl} = -2\langle\Delta\varepsilon_{hkl}(\psi)\rangle\tan\theta_{0,hkl}. \tag{1}$$

Neglecting the occurrence of macroscopic elastic anisotropy (in the specimen frame of reference; e.g. due to texture, anisotropic grain interaction [2], ….), the hkl- and ψ-dependent elastic macrostrain measured according to eq. (1) is related with the macrostress $\sigma_{\parallel}$ by [2]

$$\left\langle\varepsilon_{hkl}(\psi)\right\rangle = 2S_1^{hkl}\sigma_{\parallel} + \tfrac{1}{2}S_2^{hkl}\sigma_{\parallel}\sin^2\psi = \left\langle\varepsilon_{hkl}(0°)\right\rangle + \left(\left\langle\varepsilon_{hkl}(90°)\right\rangle - \left\langle\varepsilon_{hkl}(0°)\right\rangle\right)\sin^2\psi, \tag{2}$$

with S_1^{hkl} and $\tfrac{1}{2}S_2^{hkl}$ as the hkl-dependent X-ray elastic constants (XECs). These XECs can be regarded as averages of certain single-crystal elastic constants (SECs) along the direction of the diffraction vector (in the crystal's frame of reference) according to $S_1^{hkl} = \langle-\nu/E\rangle^{hkl}$ and $\tfrac{1}{2}S_2^{hkl} = \langle(1+\nu)/E\rangle^{hkl}$ (with E being the Young's modulus, and with ν being the Poisson ratio), where the type of averaging depends on the type of grain interaction. S_1^{hkl} and $\tfrac{1}{2}S_2^{hkl}$ can straightforwardly be calculated for certain types of (here isotropic) grain interaction from the single-crystal elastic constants [2], in particular for the extreme cases of Voigt- and Reuss-type grain interactions. For the Voigt case the XECs S_1^V and $\tfrac{1}{2}S_2^V$ are constants independent from hkl. For the Reuss case the XECs $S_1^{R,hkl}$ and $\tfrac{1}{2}S_2^{R,hkl}$ can be expressed as 4th-order polynomials in the components x_1, x_2 and x_3 of a unit vector $\mathbf{x}(hkl)$ parallel to the diffraction vector of the peak hkl (expressed with respect to the crystal frame of reference, a Cartesian coordinate system defined in a given way with respect to the crystallographic coordinate system with the basis vectors $\mathbf{a}$, $\mathbf{b}$ and $\mathbf{c}$):

$$S_1^{R,hkl} = R_{1,ijpq}^R x_i x_j x_p x_q \quad\text{and}\quad S_2^{R,hkl} = R_{2,ijpq}^R x_i x_j x_p x_q, \tag{3}$$

applying the Einstein summation convention. In eq. (3) both polynomials are symmetry invariant with respect to the crystal class, and the coefficients $R_{(1,2),ijpq}^R$ present combinations of SECs. The $R_{(1,2),ijpq}^R$ coefficients are equal for an arbitrary permutation of i, j, p and q.

It has been suggested that for an intermediate character of grain interaction, one may employ some weighted averages of the Reuss type and Voigt type XECs (formulas given in ref. [5]),

$$S_{1,2}^{hkl} = wS_{1,2}^V + (1-w)S_{1,2}^{R,hkl}, \tag{4}$$

with an hkl-independent weighing factor w ($0 \leq w \leq 1$), which may be determined by fitting on the basis of data pertaining to different hkl. Due to the hkl-independent S_1^V and $\tfrac{1}{2}S_2^V$, and

in view of eq. (3), also the overall $S_{1,2}^{hkl}$ in eq. (4) can be expressed as 4th-order polynomials in x_1, x_2, and x_3, e.g. with the polynomial coefficients $R_{1,ijpq}$ and $R_{2,ijpq}$, analogously to eq. (3):

$$S_1^{hkl} = R_{1,ijpq}x_i x_j x_p x_q \quad \text{and} \quad S_2^{hkl} = R_{2,ijpq}x_i x_j x_p x_q. \tag{5}$$

Irrespective of the relatively complex formulas leading to eq. (5), it is obviously expected that the change in macrostrain with ψ varying from 0° to 90° amounting $\langle \varepsilon_{hkl}(90°) \rangle - \langle \varepsilon_{hkl}(0°) \rangle = \frac{1}{2}S_2^{hkl}\sigma_{\parallel}$ (this quantity is called for simplicity in the following *the macrostrain*) will be large if the direction of the diffraction vector given by **x**(*hkl*) in the crystal frame of reference corresponds to an elastically compliant direction of the crystal and small if a stiff direction is concerned.

The strain in the specimen along the diffraction vector is usually not constant but is distributed. The variance of the microstrain distribution along the diffraction vector, $\langle (\varepsilon_{hkl} - \langle \varepsilon_{hkl} \rangle)^2 \rangle = \langle (\Delta\varepsilon_{hkl})^2 \rangle$ (a possible ψ dependence of the variance is not indicated here, e.g. by $\langle (\Delta\varepsilon_{hkl}(\psi))^2 \rangle$ because no systematic variation with ψ was found), appears as microstrain broadening on the diffraction scale as (strain is assumed to be constant in each coherently diffracting crystallite)

$$\langle (\Delta 2\theta_{hkl})^2 \rangle = 4\tan^2\theta_{0,hkl}\langle (\Delta\varepsilon_{hkl})^2 \rangle. \tag{6}$$

Like it is the case for $S_{1,2}^{hkl}$ under the above-mentioned assumptions (cf. eq. (5)), also the variance $\langle (\Delta\varepsilon_{hkl})^2 \rangle$ can be expressed as a symmetry-invariant 4th-order polynomial in x_1, x_2, and x_3:

$$\langle (\Delta\varepsilon_{hkl})^2 \rangle = Z_{ijpq}x_i x_j x_p x_q, \tag{7}$$

where, again, like in eq. (3) and eq. (5), the Z_{ijpq} coefficients are equal for an arbitrary permutation of i, j, p, and q. These Z_{ijpq} coefficients are connected with the variances and/or the covariances of the distribution of the strain-tensor components over the diffracting grains formulated with respect to the crystal frame of reference as used for the vector **x**(*hkl*) [6]. In the course of a phenomenological assessment of the microstrain broadening like in the course of a Rietveld refinement, the Z_{ijpq} coefficients can be refined as parameters.

It is noted that in practice, the microstrain broadening often exhibits a pseudo-Voigt like shape, which has no finite variance. In order to avoid this complication instead of the variance of the line broadening or of the microstrain along the diffraction vector in eq. (6) and eq. (7), the corresponding squared Full-Width at Half Maxima (FWHMs), $B_{\Delta 2\theta_{hkl}}^2$ and $B_{\Delta\varepsilon_{hkl}}^2$, will be employed. The corresponding coefficients in eq. (7) then are indicated by Z_{ijpq}^B.

Values for the Z_{ijpq} or the Z_{ijpq}^B parameters can be derived for different types of models for the microstrain distribution pertaining to various physical origins: different types of isotropic field-tensor variations connected with strain via anisotropic property tensors [7], microstrains due to dislocations [8, 9], or thermal microstrain estimated employing maximum entropy method [10]. Refs. [7-10] deal, in particular, with cases of microstress distributions and corresponding microstrain distributions connected with each other via the intrinsic elastic anisotropy. In all these cases the elastic anisotropy in some way affects the Z_{ijpq} coefficients and determines their values.

In general, without adopting a particular physical model for the microstrain distribution, like [7-10], one may expect that peaks *hkl* show in particular large microstrain broadening, if the crystal direction parallel to the diffraction vector is in particular elastically compliant. This

statement is analogous to that below eq. (5) concerning the $\mathbf{x}(hkl)$ dependence of $\frac{1}{2} S_2^{hkl} \sigma_\parallel$. Thus, if anisotropy of the microstrain broadening is determined by the anisotropy of the single-crystal elastic compliance, the $\mathbf{x}(hkl)$ dependency of $B_{\Delta\varepsilon_{hkl}}^2$ should be similar to that of $\frac{1}{2} S_2^{hkl} \sigma_\parallel$.

Experimental

A massive, polycrystalline Fe_3C layer (thickness 4.6 μm) was grown on a plate-like α-iron substrate (thickness 1 mm) by a dedicated nitrocarburisation procedure [3, 4]. High-resolution X-ray powder-diffraction experiments on this layer were performed at HASYLAB, Hamburg, Germany. Station B2 was equipped with a Eulerian cradle and operated with a wavelength of 0.79323 Å, which is sufficiently small to ensure negligible absorption of radiation within the Fe_3C layer. An analyser crystal in the diffracted beam ensured narrow instrumental profiles, which were determined by measuring peaks of a LaB_6 (NIST SRM660a) standard sample. During the measurements both specimens (Fe_3C and LaB_6) were rotated around their surface normal to achieve better crystallite statistics. A selected number of peaks were measured at different sample tilting angles ψ for both specimens.

Data evaluation was carried out with the *TOPAS* [11] software. The instrumental profile was determined by fitting of split-Pseudo Voigt functions to the LaB_6 peaks. The instrumental profile shape and width parameters pertaining to different Bragg angles were interpolated by means of polynomials to determine values at arbitrary Bragg angles. On this basis the peak profiles recorded from the Fe_3C layer were evaluated by convoluting the instrumental-profile function at the respective Bragg angle with a split pseudo-Voigt function, representing the physical line broadening, with fitted shape and width parameters. The peak positions as well as the FWHMs of the physical line broadening, $B_{\Delta 2\theta_{hkl}}$, for various hkl were the basis for the further evaluations.

Results and discussion

The ψ-dependent peak shifts had been used in order to evaluate the Fe_3C layer's state of macrostrain and macrostress [4]. To this end SECs from first-principles calculations had been used for calculation of XECs according to eq. (4), yielding a compressive (mechanical) macrostress of $\sigma_\parallel = -440$ MPa. The macrostrains $\frac{1}{2} S_2^{hkl} \sigma_\parallel = \left\langle \varepsilon_{hkl}(90°) \right\rangle - \left\langle \varepsilon_{hkl}(0°) \right\rangle$ in the $\sin^2\psi$ plots (macrostrain) according to eq. (2) vary significantly with hkl, as expected for hkl-dependent XECs. This reflects the extreme elastic anisotropy indicated by the SECs (very small C_{2323} vs. $10 \times$ larger C_{1313} and C_{1212}), which leads to the largest peak shifts from ($\psi = 0°$ to $90°$) for peaks with small h and simultaneously large k and l (indices and tensors refer to the *Pnma* setting of the cementite's crystal structure).

The line widths vary primarily (also) with hkl; slight variations with ψ occur, too, but no systematic ψ dependency can be discerned. Therefore, in the following the averaged values of the line widths recorded at $\psi = 25°$ and $37°$ are used. Further, it is assumed that the complete physical line broadening is of microstrain type. Thus, using eq. (6), using the squared FWHMs instead of the variances, one can calculate $B_{\Delta\varepsilon_{hkl}}^2$. The $B_{\Delta\varepsilon_{hkl}}^2$ values have been plot-

ted versus the $\frac{1}{2}S_2^{hkl}\sigma_{\parallel} = \left\langle \varepsilon_{hkl}(90°) \right\rangle - \left\langle \varepsilon_{hkl}(0°) \right\rangle$ in figure 1. Evidently, a clear positive correlation occurs: correlation factor of 0.80, although a few systematic outliers occur (e.g. 002). Note that this analysis is possible simply on the basis of the bare experimental data, without knowledge of values for the XECs.
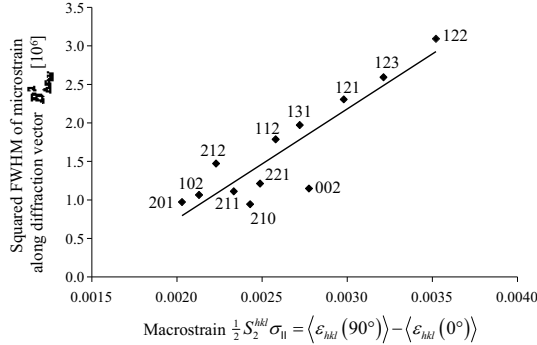

Figure 1. Comparison of the squared FWHM values of the microstrain distribution along the diffraction vector with the slopes of $sin^2\psi$ plots (macrostrain) according to eq. (2) for various hkl.
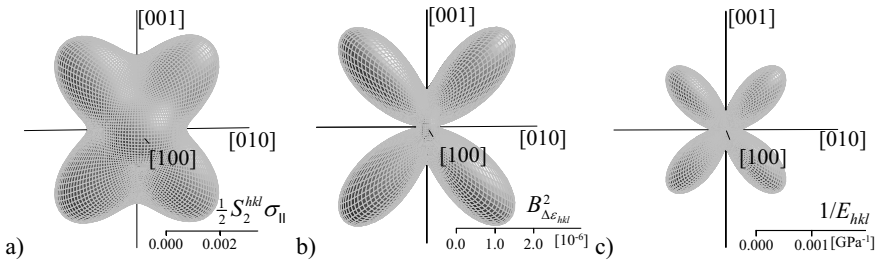

*Figure 2. (a) and (b): Tensor surfaces (drawn with Wintensor [12]) representing microstructural properties of the cementite layers as a function of the direction **x**(hkl) of the diffraction vector in the crystal coordinates: (a) slopes of the $sin^2\psi$ plots (macrostrain) and (b) squared FWHM of the microstrain distribution along the diffraction vector. The tensor surface in (c) illustrates the direction dependence of the reciprocal Young's modulus [4].*

Moreover, the similar anisotropies of the macrostrain ($\frac{1}{2}S_2^{hkl}\sigma_{\parallel} = \left\langle \varepsilon_{hkl}(90°) \right\rangle - \left\langle \varepsilon_{hkl}(0°) \right\rangle$) and of the microstrain ($B^2_{\Delta\varepsilon_{hkl}}$) in the crystal frame of reference can be illustrated on the basis of tensor surfaces representing the direction dependencies of these quantities: see figure 2. For that purpose, on the basis of the experimental data for different *hkl*, 6 different coefficients $\frac{1}{2}R^R_{2,ijpq}\sigma_{\parallel}$ representing the macrostrain were fitted on the basis of the $\frac{1}{2}S_2^{hkl}\sigma_{\parallel}$ data (eq. (5)) and analogously 6 different coefficients Z^B_{ijpq} representing the microstrain were fitted on the basis of the $B^2_{\Delta\varepsilon_{hkl}}$ data (eq. (7); using the squared FWHMs instead of the vari-

ances). The number of 6 coefficients follows from the invariance with respect to the ortho-rhombic symmetry of Fe_3C [6]. Indeed, the surfaces look qualitatively similar. They both also resemble the tensor surface describing the direction dependence of the reciprocal Young's modulus $1/E_{hkl} = S_{ijpq}x_ix_jx_px_q$ (also shown in figure 2), which demonstrates the softness of directions intermediate between [010] and [001]. This softness is a direct consequence of the small shear modulus C_{2323} mentioned above.

The remaining differences in the precise shapes of the tensor surfaces are e.g. related with the averaging necessary for going from the SECs (fig. 2c) to the XECs (contained in fig. 2b). Moreover, different models exist (and more are imaginable) for how elastic anisotropy may show up microstrain [7-10].

Conclusion

The intrinsic anisotropic elastic properties of a solid may be exhibited by the anisotropy of the observed elastic macrostrain and of elastic microstrain: Elastically compliant directions exhibit larger values of macrostrain and of microstrain than stiff directions.

References

1. Sayers, C.M., 1984, *Phil. Mag. A*, **49**, 243.

2. Welzel, U., Ligot, J., Lamparter, P., Vermeulen, A.C. & Mittemeijer, E.J., 2005, *J. Appl. Cryst.*, **38**, 1.

3. Gressmann, T., Nikolussi, M., Leineweber, A. & Mittemeijer, E.J., 2006, *Scr. Mater.*, **55**, 723.

4. Nikolussi, M., Shang, S.L., Gressmann, T., Leineweber, A. & Mittemeijer, E.J., Wang, Y. & Liu, Z.-K., 2008, *Scr. Mater.*, **59**, 814.

5. Howard, C.J. & Kisi, E.H., 1999, *J. Appl. Cryst.*, **32**, 624.

6. Leineweber, A., 2006, *J. Appl. Cryst.*, **39**, 509.

7. Leineweber, A., 2007, *J. Appl. Cryst.*, **40**, 362.

8. Ungar, T. & Tichy, G., 1999, *Appl. Phys. Lett.*, **69**, 425.

9. Leoni, M., Martinez-Garcia, J. & Scardi, P., 2007, *J. Appl. Cryst.*, **40**, 790.

10. Kreher, W. & Pompe, W., 1989, *Internal Stresses in Heterogeneous Solids* (Berlin: Akademie-Verlag).

11. TOPAS. *General Profile and Structure Analysis Software for Powder Diffraction Data* (Karlsruhe, Germany: Bruker AXS GmbH).

12. Kaminsky, W., 2004, *Wintensor* Version 1.1, Cologne, Seattle, Oxford.